GEOPHYSICS, VOL. 64, NO. 5 (SEPTEMBER-OCTOBER 1999); P. 1492–1501, 10 FIGS.

First-break timing: Arrival onset times by direct correlation

Joseph B. Molyneux* and Douglas R. Schmitt‡

ABSTRACT

In attenuating media, pulse characteristics evolve with propagation distance and saturation or pressure-dependent changes in rock properties. This nonstationarity of the waveform complicates determination of meaningful traveltimes. As a result, depending on the time-picking criteria used, substantially different values of interval velocity can be obtained. This problem is particularly severe in high-frequency laboratory time-of-flight measurements on porous rock. A potentially less ambiguous measure of wave speed is the signal velocity that is calculated using the pulse onset time. Here, a semiautomated method is developed to determine this onset time in high-fidelity, pressure-dependent core measurements. The greatest value of Pearson's correlation coefficient between segments of observed waveforms near the pulse onset and at an appropriate reference serves as the time determination criterion. Tests of the method on artificial data suggest the signal velocity may be determined to better than 0.3% for −60 dB noise or 1.2% for −37 dB noise. A real data set is tested, comprised of a series of ultrasonic (1 MHz) velocity measurements in microcracked rock to confining pressures of 300 MPa (∼45,000 psi). At the lowest confining pressure, where attenuation is greatest, signal onset and more conventionally derived traveltimes differ by more than 4%. This large discrepancy illustrates that care should be exercised when determining velocity in such attenuating materials. Conversely, the consistency of waveform attributes, such as the difference between the onset time and the first peak time or the apparent quality factor, is useful when estimating intrinsic material velocities in low-porosity, microcracked carbonate and metamorphic rocks at high confining pressures.

INTRODUCTION

The time of the first break is used in velocity measurements ranging from elementary refraction profiling to the most sophisticated tomographic inversions of first arrivals. The term first break is not precisely defined, and it is relevant to ask which feature of the arriving waveform provides the best measure of the time of flight. Which is more important: the initial time of onset or a more readily identifiable characteristic, such as the first peak? If the propagating wavelet shape does not evolve with time, the determination of interval velocities from either of these criteria yields identical results. However, in the real world both intrinsic absorption and scattering contribute to the signal attenuation, which manifests itself as a broadening in time of a propagating wavelet. In some measurements the onset times differ by several percent from those determined with a first peak. In such situations, this discrepancy ceases to be of only academic interest. Unfortunately, it is not immediately obvious which waveform feature provides the most representative measure of material properties or physical structure.

For any propagation mode (i.e., compressional, shear, Rayleigh, etc.) the wave speed is the quotient of propagation distance with time of flight. In real media, these wave speeds depend on frequency. This dispersion results from a combination of intrinsic absorption and scattering effects (e.g., Brillouin, 1960; Futterman, 1962). Because both phase and group velocities depend on frequency, a band-limited disturbance changes form as it propagates. This is of particular concern when the attenuation of the sample under study changes with varying states of saturation (Bourbie and Zinszner, 1987) or confining pressures, as in the present investigation.

Signal velocity is another important measure. Sommerfeld (in Brillouin, 1960) defines the signal onset time, used in calculating the signal velocity, as the time at which the energy of the signal is first detectable. One advantage of using the onset time is that it is less influenced by dispersion-dependent waveform

Presented at the 67th Annual Meeting, Society of Exploration Geophysicists. Manuscript received by the Editor March 17, 1998; revised manuscript received January 14, 1999.
*Formerly Department of Physics, University of Alberta, Edmonton, Alberta T6G 2J1, Canada; currenlty Mobil Oil Canada Ltd., 330 Fifth Ave. S.W., Calgary, Alberta T2P 2J7, Canada. E-mail: joe_b_molyneux@email.mobil.com.
‡Department of Physics, University of Alberta, Edmonton, Alberta T6G 2J1, Canada. E-mail: doug@phys.ualberta.ca.

modification. Onset traveltimes may then be more consistent than those that rely on the picking of some later waveform feature likely to be influenced by dispersion.

The overall question of which velocity definition is most useful will not be answered in this contribution, which instead focuses on the technical issue of accurately determining Sommerfeld's definition of the signal velocity in high-fidelity waveforms acquired in laboratory experiments. Below, earlier first-break picking schemes are reviewed. A strategy to measure the onset times is described and implemented with a suite of pressure-dependent ultrasonic waveforms (Figure 1) acquired in the laboratory. The results illustrate how critical the definition of the first break is in attenuating media. Finally, the absorptive and transit time characteristics of a candidate rock are compared; these reveal additional criteria with which to judge the quality of intrinsic velocity determinations in materials containing microcrack porosity.

PREVIOUS METHODS

Seismic traveltime picking

Modern seismic studies require that large data volumes be analyzed. Manual traveltime picking is slow and subject to inconsistent operator bias and error. To attempt to circumvent these shortcomings, several automated picking schemes have been developed, and these may be classified as either running window or coherency methods.

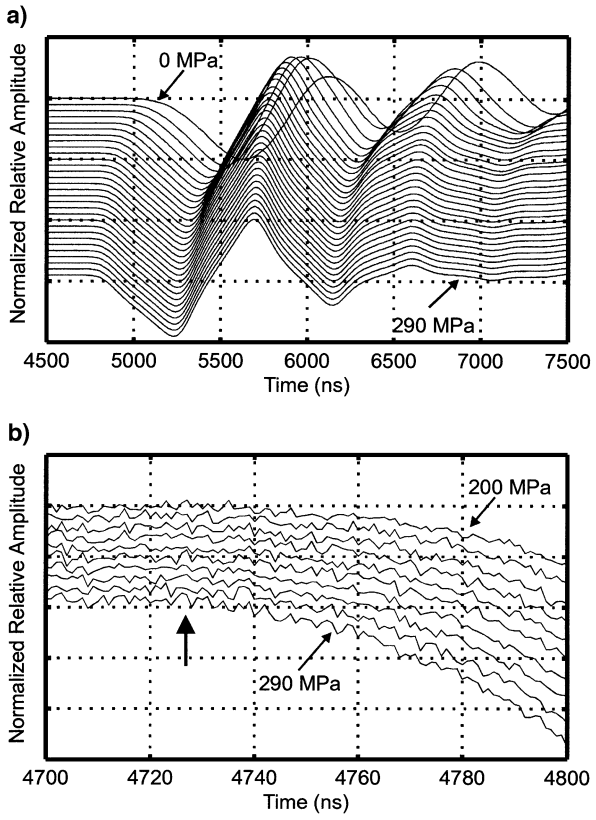

FIG. 1. (a) Typical transmitted ultrasonic waveforms acquired over a range of confining pressures to 290 MPa through a rock cylinder. Waveforms are vertically offset according to the pressure at which they were obtained for viewing convenience. (b) Twenty times vertical exaggeration of a subset of the waveforms in (a) with confining pressures from 200 to 290 MPa. The arrow indicates the manually picked arrival onset time for the 290-MPa reference template waveform. Amplitudes are normalized with respect to each waveform's greatest amplitude.

In the former, certain characteristics are repeatedly calculated within successive sections of the time series, producing a time-dependent function. The onset time is usually identified by an obvious change in the behavior of this function. Such running window methods proficiently identify changing waveform character. The averaging inherent to these techniques smooths the calculated response and complicates traveltime determination. In one example, Boschetti et al. (1996) calculate the fractal dimension of time windows along a seismic signal. This method relies on the empirical observation that the fractal dimension (Boschetti et al., 1996) of a coherent signal differs substantially from that of prearrival noise. The first onset time is indicated by a reduction of the fractal dimension, and such a change in character is visible in even the noisiest data. However, this measure does not change abruptly, and there remain potential timing ambiguities.

A second method relies on using the coherence characteristics between traces. Coherency-based methods rely on a quantitative comparison of an object and a shifting reference waveform. The time of waveform arrival is when the measure of the quality of match is maximum. Such correlation or convolution methods presumably yield group velocities as the properties of the waveform as a whole are compared. In a refraction seismic study, Peraldi and Clement (1972) crosscorrelate a reference waveform, with an ostensibly known arrival time, to other traces in the data set. This method assumes the waveforms in each trace are reasonably similar to the reference; the maxima of the crosscorrelation indicate the shifts of their traveltimes with respect to the reference waveform. Other coherency-based timing methods are found in the literature (Ervin et al., 1983; Ramananantoandro and Beritsas, 1987; Su and Dziewonski, 1992). Additional picking methodologies use both running window and coherence methodologies (Hatherly, 1982; Coppen, 1985; Gelchinsky and Shtivelman, 1986; Spagnolini, 1991; and Murat and Rudman, 1992).

Development of a truly causal first arrival in theoretical studies is often hindered by the deficiencies intrinsic to the modeling itself. Often, frequency-domain filtering of a trace causes the signal to become noncausal in the sense that a small amount of energy leaks into times prior to the first arrival. This effect is noted by Ricker (1953) who, in a predigital age, suggested that one can never find a portion of the signal with a zero amplitude such that the arrival first kick can be defined. As a practical result, Schmidt and Muller (1986) and Gudmundsson (1996) define the onset of calculated model signals to occur when the amplitudes exceed an arbitrary level that they choose as the time to 1/100 and 1/8, respectively, of the maximum amplitude.

Recently, Boschetti et al. (1996) quantitatively compared a number of the above techniques. However, in most of these studies the automatic first-break times were compared only to those determined manually. No objective measure of the picking accuracy was presented.

Laboratory traveltime measurement

The primary difference between waveforms acquired in laboratory settings and those acquired in the field is that the

laboratory data are usually less contaminated with noise. Despite this, the picking of accurate transit times in laboratory samples is particularly critical, given the high velocities (1–8 km/s) and short transit times (a few microseconds). In the earth sciences, the pulse overlap method described by Birch (1960) is traditionally used to find velocity in rock samples (e.g., Christiansen, 1965; Fountain et al., 1990). Ultrasonic pulses propagate simultaneously through a sample and a delay-line column of mercury. Both transmitted signals are displayed on an oscilloscope, and the length of the mercury delay line is varied until the two signals overlap. Since the velocity of the mercury column is presumed known, the transit time through the sample is easily derived. In a similar manner, pulse echo overlap methods (e.g., Papadakis, 1990) involve finding the time delay between the first arrival of a pulse and its multiple reflections. Here, the oscilloscope time base is altered until a multiply reflected arrival overlaps the earlier arrival. The time sweep then provides a measure of the traveltime. In many respects both of these methods are similar to the digital correlation techniques.

Alternatively, the first-peak time of an input pulse as it propagates through a cored rock sample is often measured (King, 1966; Kern and Richter, 1981). The transit time through the recording apparatus is corrected by measuring the difference in the timing of the first-peak amplitude when the rock core lies between the transducers relative to when the transducers are placed directly in contact. Such a measurement is predicated on the observation that the waveform is stationary at elevated pressures and as such consistently monitors traveltime differences with increasing pressure. However, as indicated in Figure 1, waveforms acquired at low pressures can significantly differ from those at high pressure. This can result in substantial differences between the traveltime measured from signal onset and first peak.

Although the essential concepts of velocity determination apply to both seismic and ultrasonic laboratory applications, in practice one important difference is that the latter is usually less contaminated with noise. Further, such signals are also recorded at high sampling rates such that the Nyquist frequency is large relative to their frequency bandwidth. Such high-fidelity signals are advantageous in that they allow greater accuracy in the determination of the signal onset. In this context the running window approaches, although useful in coarsely sampled and noisy seismic data, are inappropriate because of their inherent smoothing. The waveform comparison methods unambiguously identify a transit time but suffer in that they assume stationary waveforms. Here, we present an alternative onset-time determination that uses a correlation of the shape of the waveform but only in the vicinity of the signal onset, minimizing the effect of dispersion.

ONSET TIME DETERMINATION

Direct correlation

In this section, the direct correlation traveltime determination technique is described and then tested on synthetic data. The method relies on the comparison of waveform shapes near the signal onset, examples of which are shown in Figure 1b. The method is analogous to hodogram analysis (crossplot of the amplitudes of two associated traces) usually employed, for example, to azimuth orient and rotate downhole three-component geophone seismic data (e.g., Kebaili and Schmitt, 1996). The crossplot of two well-correlated waveform segments appears linear.

A simple example illustrates the picking methodology. A reference template X (Figure 2a) includes the signal onset whose time is presumably known. The signal onset time of the

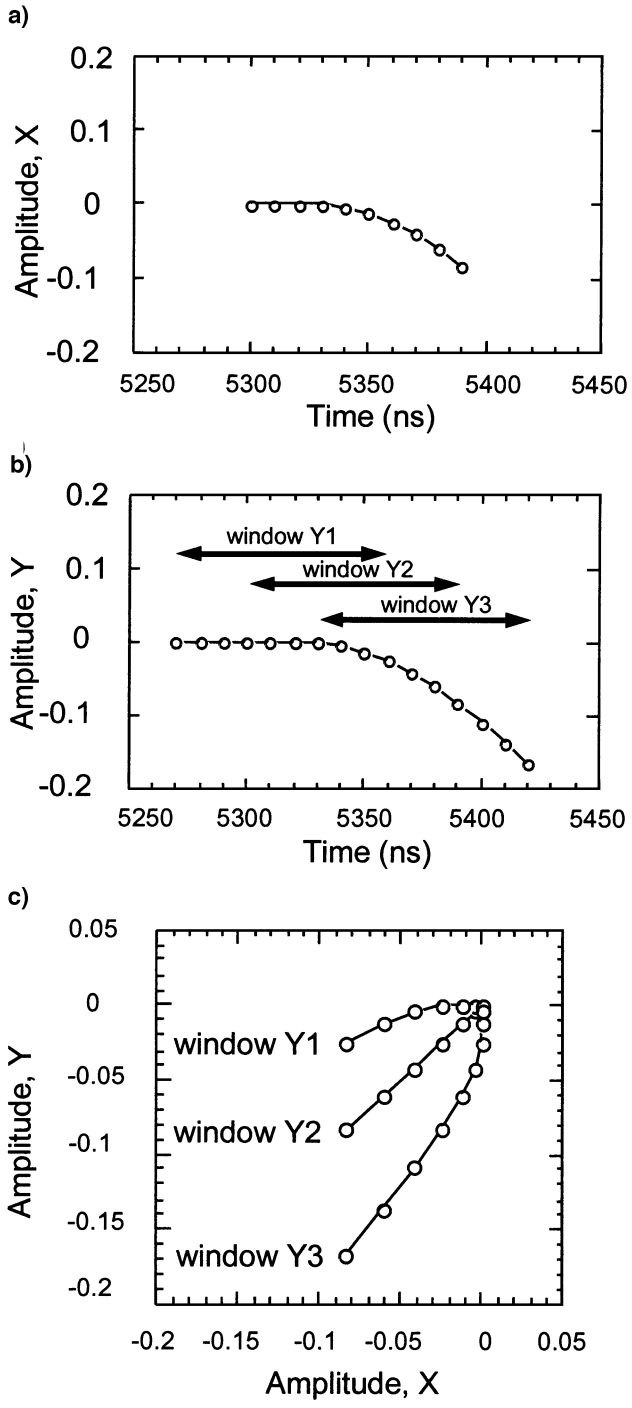

FIG. 2. Illustration of the direct correlation procedure. (a) Reference segment X in the vicinity of its known onset time. (b) Positions of three time windows relative to the amplitudes of the object waveform Y. The windows are of the same length as X and their corresponding time series, denoted $Y1$, $Y2$, and $Y3$ in the text. (c) Hodograms of $Y1$, $Y2$, and $Y3$ versus reference template X.

object waveform Y relative to that of the reference waveform X is to be found. Three separate waveform segments of the object trace Y are shown in Figure 2b. Crossplots of these object segments with the reference (Figure 2c) display a range of behaviors, but only the crossplot with the center window $Y2$ is linear. The nonlinear crossplots of $Y1$ and $Y3$, which are advanced or retarded with respect to X, simply indicate that their shapes differ from the template X. In contrast, the linearity of the middle crossplot for $Y2$ suggests its shape is most similar to the template; consequently, the time shift of window $Y2$ relative to template X yields the difference in their onset traveltimes.

A means to provide an objective measure of the linearity in the crossplots is required. The simplest and best-known measure of linearity in this context is Pearson's coefficient of correlation (Taylor, 1982), here given as $r(\tau)$:

$$r(\tau) = \frac{n\sum_{t=0}^{t=n} X(t)Y(t+\tau) - \sum_{t=0}^{t=n} X(t)\sum_{t=0}^{t=n} Y(t+\tau)}{\sqrt{n\sum_{t=0}^{t=n} X(t)^2 - \left(\sum_{t=0}^{t=n} X(t)\right)^2}\sqrt{n\sum_{t=0}^{t=n} Y(t+\tau)^2 - \left(\sum_{t=0}^{t=n} Y(t+\tau)\right)^2}}, \quad (1)$$

where X is a discrete vector of the template amplitudes n samples in length and Y is a trial segment of the object waveform of the same length. The Pearson correlation coefficient, $r(\tau)$, is calculated for Y shifted along the length of the object waveform by a series of discrete time shifts, τ. A value of $r(\tau) = 1$ indicates perfect positive linear correlation between X and Y, meaning both share the same shape. A value of $r = 0$ indicates no correlation, meaning in this context that the shapes of the curves differ; $r = -1$ indicates an anticorrelation—two curves of the same shape but with opposite polarity. Proximity of $r(\tau)$ to unity suggests a good correlation of shapes between the waveforms $X(t)$ and $Y(t+\tau)$, with the τ value at which $r(\tau)$ is maximum indicating the most appropriate time shift. An example of a calculated $r(\tau)$ versus τ for two real waveforms taken from Figure 1 is given in Figure 3. The shift that best matches the reference template occurs at 61 ns.

Validity of the crossplot technique

Our picking method is based on the assumption that two similarly shaped waveform segments with the same onset time have a linear crossplot. This will be tested by examining a simple model. Generally, a sufficiently short time window following the signal onset can be approximated by a Taylor expansion such that

$$X(t) = a_0 + a_1 t + a_2 t^2, \quad (2)$$

where $t = 0$ is the time of the signal onset and a_0, a_1, and a_2 are polynomial coefficients, with a_0 the dc offset. For purposes of this model, the object signal $Y(t)$ is similarly described with polynomial coefficients b_0, b_1, and b_2. The validity of this parameterization of the waveform is based on direct observation of waveform shapes. A least-squares regression analysis of observed laboratory waveform amplitudes (Figure 1) immediately following the manually picked onset time is quadratic with a correlation coefficient better than 0.999 for 140-ns-long time windows.

The crossplot of two quadratics of identical onset time but defined by different polynomial coefficients is nonlinear according to

$$Y(t) = \alpha + \beta t + \delta X(t), \quad (3)$$

where

$$\alpha = b_0 - \frac{b_2 a_0}{a_2},$$

$$\beta = b_1 - \frac{b_2 a_1}{a_2}, \quad (4)$$

and

$$\delta = \frac{b_2}{a_2}.$$

For a simple linear time relationship between $Y(t)$ and $X(t)$, the βt term [equation (3)] should be much less than $Y(t)$. For each of the real traces, second-order polynomials were fitted to the first 140 ns of data immediately after the manually picked onset of signal. For example, a crossplot between polynomial descriptions of the real waveforms recorded at 290 and 0 MPa confining pressure is displayed (Figure 4a,b). Using the same 290-MPa polynomial template, $X(t)$, and second-order polynomial descriptions of all the real waveforms, the percentage contribution of the nonlinear βt term to each crossplot is calculated and averaged over the 140-ns trend (Figure 4c). Where the linear coefficient of the crossplots drops to values less than $\sim$0.9996, βt contributes to more than 20% of $X(t)$ (Figure 4c,d).

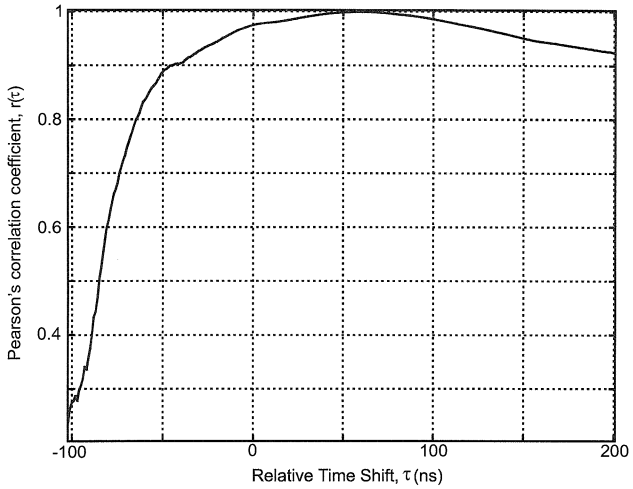

FIG. 3. Example of calculated Pearson's correlation coefficient $r(\tau)$ versus relative time shift τ for the 130- and 290-MPa waveforms.

Empirically, the observed waveforms after the first break are second-order polynomials ($r > 0.999$) over short time windows (140 ns), and the resulting crossplots are effectively linear ($r > 0.999$). This high linearity over a wide range of waveform shapes allows substantial latitude in the selection of the reference $X(t)$. Further, deviation from linearity correlates to the dominance of the βt term in equation (3) (Figure 4c,d).

Evaluation on synthetic data

The practical application of mathematical Q filters results in noncausal waveforms. Thus, it is difficult to calculate model waveforms that retain a distinct signal onset. Here, to evaluate the accuracy of the time determination procedure, a synthetic data set was derived from the real traces of Figure 1. To provide a meaningful test, these synthetics have known arrival times, known noise levels, and a character similar to the real data. To this end, the synthetic waveforms were produced by a spline fit to the real waveforms of Figure 1. All amplitudes prior to the manually picked first-arrival position were set to zero. The average noise levels of the data set, as characterized from the real data over a 300-ns-long preonset time window, were approximately −60 dB lower than the amplitude of the first amplitude minima. This noise amplitude was normally distributed. The temporal component of the noise was evaluated from a 51-point running window of the amplitude residuals between the real and smooth spline-fitted data for the noisiest trace tested (−52 dB)—that recorded at atmospheric pressure. The prearrival noise sampled with the 51-point moving window ($\sim$ −50 dB) is consistent with the results measured with a 300-data-point window (−52 dB) (Figure 5). Further, the moving window analysis illustrates that the noise remains approximately constant along the trace, indicating its stationary nature. Similarly described random white noise was then added to each noise-free trace to produce the synthetic data (Figure 6). The advantage of this procedure is that the resulting traces are similar in form and noise level to the real data but have onset arrival times that are known a priori. The onset of energy time was 4727 ns for the 290-MPa synthetic reference waveform.

A variety of tests were carried out to optimize the method. First, the waveform recorded at 290 MPa confining pressure, which exhibited the lowest level of preonset noise, was used as the template to easily pick its first arrival and to minimize noise contamination in all subsequent crossplots. Picking error was determined from the variation between the true onset

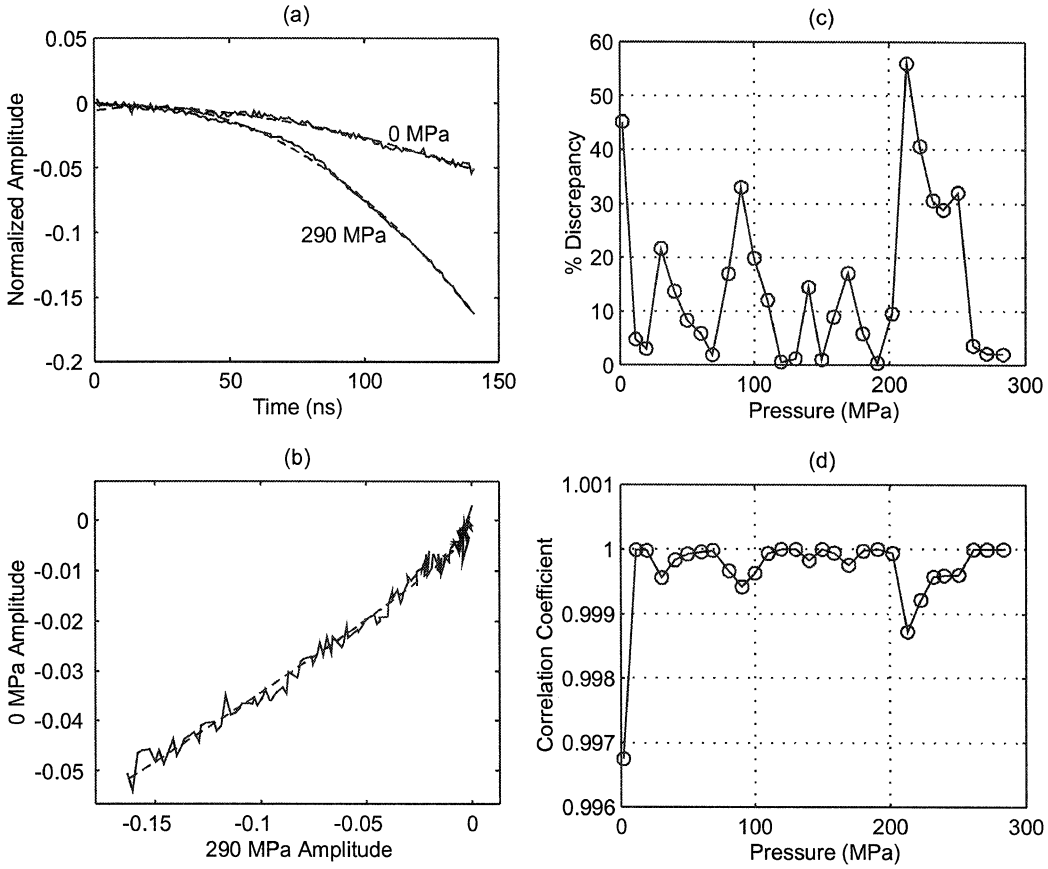

FIG. 4. Linearity of polynomial crossplots. (a) A plot describing 140-ns waveforms immediately after their first breaks for real waveforms measured at 290 MPa and atmospheric pressure (solid lines) and their respective second-order polynomial best fits (dashed lines). (b) Crossplot of the two 140-ns-long waveforms (solid line) and their respective polynomial crossplot (dashed line). (c) Average $\beta t / Y(t)$ percent discrepancy versus pressure for the polynomial descriptions of the waveforms tested. (d) Linearity of the polynomial crossplots versus pressure for the polynomial descriptions of the waveforms tested.

times and those determined by the Pearson correlation procedure. The most accurate results were obtained if the template commenced at least 20 ns before the signal onset. This preonset segment unambiguously characterizes the template as a wave segment containing the first-break information. A window length approximately one-seventh the dominant period of the signal (160-ns template length) minimized the total picking error (the magnitude addition of the mean and standard deviation of error) (Figure 7). Such a template yielded a mean and standard deviation of error between the actual onset arrival times and those picked with the Pearson correlation negative 2 and 6 ns, respectively. This 8-ns picking error represents <0.2% of the approximate 4800-ns propagation traveltime. Elevated noise levels increase this picking error, so that at noise levels of −37 dB the picking error is ∼60 ns (∼1.2%) (Figure 8).

One interesting problem is that the Pearson correlation pick tended to be later than the actual traveltime, as indicated by the systematic negative mean in Figure 8. This bias results from the leveraging effect of the higher amplitudes of $Y3$ on the crossplot (Figure 2).

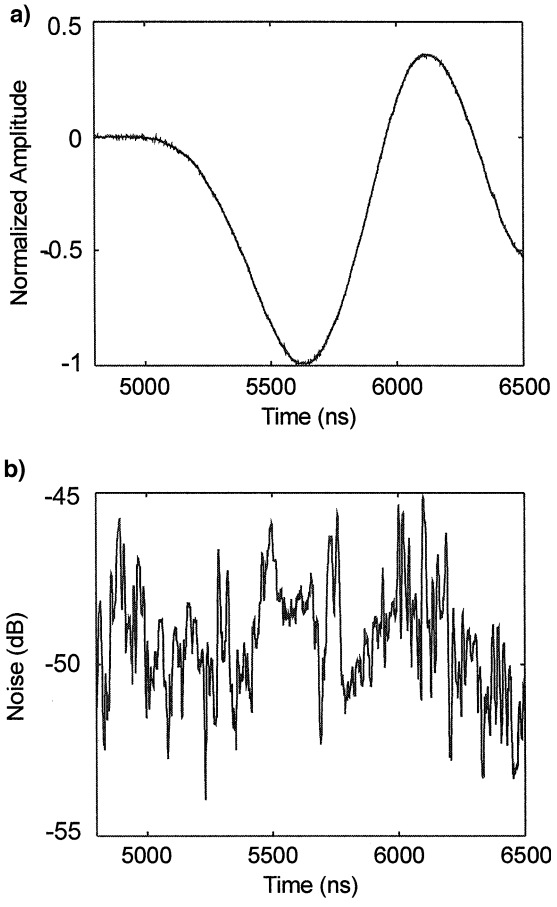

FIG. 5. Temporal noise characteristics of the experimental signal recorded at atmospheric pressure. (a) The wave segment evaluated, with the onset of signal at ∼4985 ns. (b) Temporal variation of noise calculated from a 51-point running window. Noise levels (in decibels) are calculated in comparison to the absolute amplitude of the first waveform minimum.

LABORATORY TESTS

Real laboratory waveforms (Figure 1) have already been presented in the error estimation. The experimental acquisition of these waveforms is now described.

The traveltime determination procedure was developed to aid P-wave velocity measurements in metamorphic rocks studied as part of the LITHOPROBE TransHudson Transect (Hajnal et al., 1996). The velocity of metamorphic and well-consolidated sedimentary rocks is very nonlinear with pressure because of the existence of high-aspect-ratio, cracklike, pressure-dependent porosity. Velocities are often measured at high pressure, when much of this porosity is closed, to provide an estimate of the crack-free in-situ properties (Birch, 1961). This microcrack problem is particularly severe in metamorphic rock samples (Meglis et al., 1996); thus, each sample measurement is carried out to pressures of 300 MPa (∼45,000 psi) to record intrinsic rock properties. The traveltime picking method was applied to over 150 different samples, each with over 60 waveforms.

The experimental configuration is shown in Figure 9. Two 1-MHz resonant frequency piezoelectric transducers are attached directly to the parallel flattened ends (±0.02 mm) of 2.54-cm-diameter cylindrical core plugs. The core plug used here is 31.70 cm long. The transmitting transducer is activated by a square wave pulse and the received output is digitized by a high-speed digital oscilloscope (1-ns sampling interval) and stored to disc. The core plug is dried under vacuum, then hermetically sealed in flexible urethane before being placed in the pressure vessel. The plug is then subjected to increasing pressure from standard conditions to 300 MPa in steps of 10 MPa. A waveform is acquired at each step, producing a suite of pressure-dependent waveforms such as shown in Figure 1. No electronic filtering or amplification was applied to the received signal, and frequency-domain bandpass filtering was not applied to the data because removal of even low-amplitude frequency components may smooth the relatively abrupt onset. Causal time-domain filtering was not attempted. The progressive decrease of the onset traveltimes with change in pressure is common in metamorphic velocity studies. Also, the waveforms recorded at low confining pressure are much broader in shape than those recorded at greater pressures.

The apparent quality factor, Q, was measured using spectral ratios (e.g., Toksoz et al., 1979) over the entire pressure range to 300 MPa. In this method the ratio of the Fourier amplitude spectra $A_1(f)$ and $A_2(f)$ of the pulse transmitted through a standard and the rock sample, respectively, is used. The apparent Q was determined from the slope of the spectral ratio

$$ln\frac{A_2(f)}{A_1(f)} = \frac{-\pi(t_2 - t_1)}{Q} f, \tag{5}$$

where f is the frequency in Hertz and t_1 and t_2 are the propagation times through the aluminum standard and the rock core, respectively. The standard was an aluminum cylinder whose dimensions were identical to those of the rock sample. The aluminum cylinder is assumed to have negligible attenuation at ultrasonic frequencies, with $Q > 120\,000$ for frequencies >100 kHz (Zemanek and Rudnick, 1961). This spectral-ratio method inherently assumes that Q is constant over the 0.5 to

1.5-MHz bandwidth of the ultrasonic wave packet (Ganley and Kanasewich, 1980).

RESULTS AND DISCUSSION

The onset times of the ultrasonic data of Figure 1 were determined manually and using the Pearson correlation method. The template, X, commenced 20 ns before the manually picked first arrival and 140 ns after, in analogy to the synthetic data. Altering this length of template deteriorated the Pearson correlation picking accuracy with respect to the trend of the manually picked arrivals. The manually determined transit times display significantly more scatter than those eventually determined with the Pearson correlation, relative to a presumably smooth trend of velocity with pressure (Figure 10a). Although this attribute does not in itself prove that the computer-picked times are correct, it does suggest that the method is less error prone than more subjective manual determinations. The times measured by the Pearson correlation method are also compared to those provided by other potential automatic techniques (Figure 10b): the first-amplitude extremum time (e.g., King, 1966; Gudmundsson, 1996), the crosscorrelation of the whole waveform packet (e.g., Birch, 1960; Peraldi and Clement, 1972), and the crosscorrelation of amplitude envelopes. In all cases the 290-MPa waveform was used as the reference because it contained low noise contamination. The amplitude envelope measurement, calculated using the Hilbert transform (Taner et al., 1979), is included as an estimate of the wave-packet propagation, i.e., the group velocity. All results are displayed as a differential time of onset (i.e., relative to that of the 290-MPa template waveform). An absolute measure of the total traveltime is given by adding the manually picked onset time of the low-noise 290-MPa template. The template onset time is subjectively estimated within ±5 ns which, added to the previous 8-ns error determined from the synthetic model, results in a 13-ns picking error. This picking error translates to less than 1/100th of the dominant signal period, or specifically for a typical 4800-ns arrival time, a 0.3% error.

At the lowest hydrostatic confining pressures, below 100 MPa, the methods give dissimilar traveltimes. These differences transfer directly into the calculation of the material velocity when the sample length is divided by the traveltimes (Figure 10c). However, it is unclear which velocity property

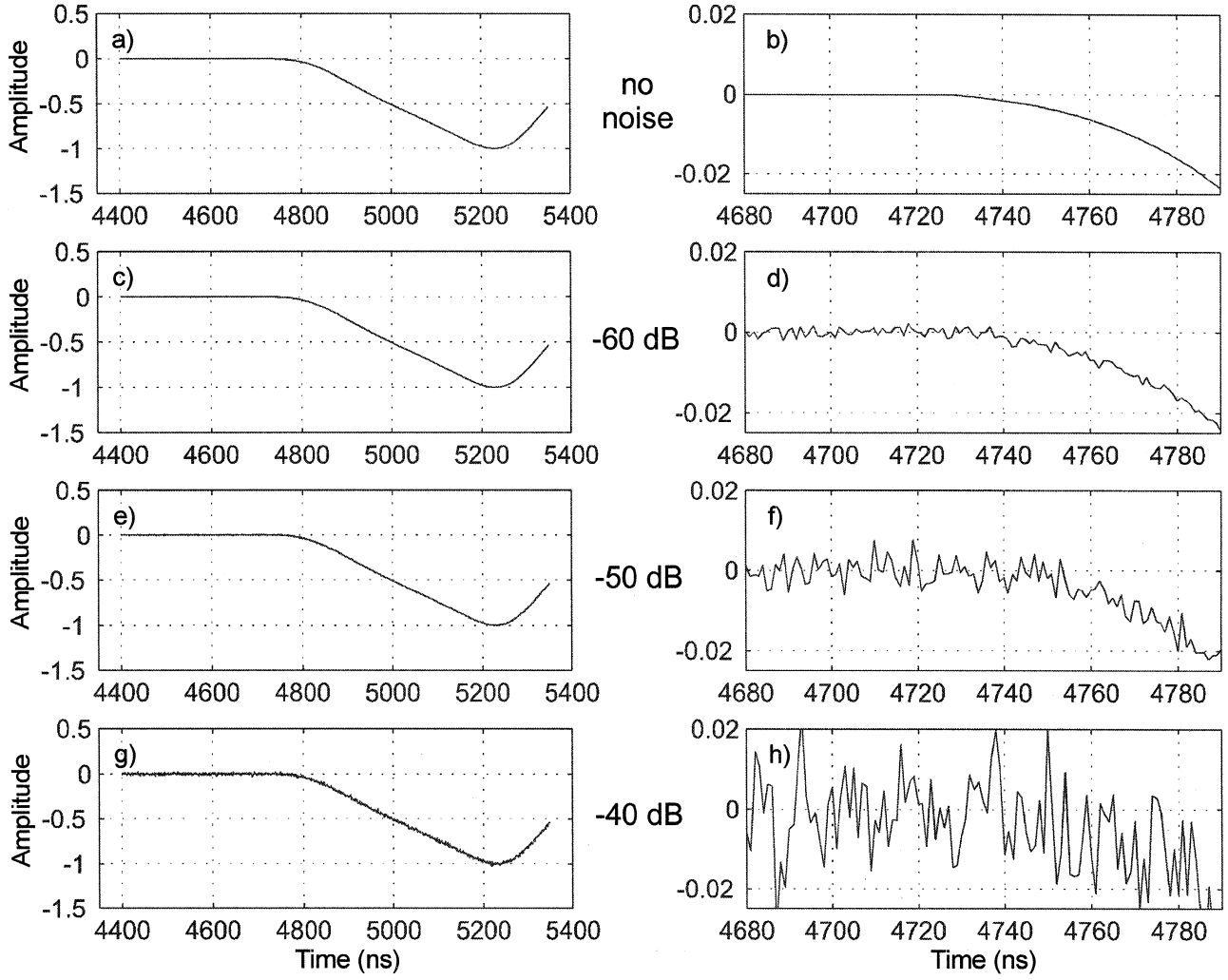

FIG. 6. Microsecond and 100-ns scale segments of the synthetic test waveforms derived from the observed 290-MPa trace with (a,b) no added noise, (c,d) low noise (−60 dB), (e,f) moderate noise (−50 dB), and (g,h) high noise (−40 dB).

best describes the medium. Above 100 MPa of confining pressure, the difference between the traveltimes remains essentially unchanged aside from random noise. This is demonstrated by the nearly constant and small percentage difference between the signal and crosscorrelation velocities above 150 MPa (Figure 10d). These observations show that the waveforms remain nearly stationary above this pressure, suggesting that attenuation and dispersion change little.

The apparent Q increases from ~6 at atmospheric pressure to nearly 40 at 300 MPa (Figure 10e). These observations agree to 150 MPa with those of Meglis et al. (1996), who attributed the attenuation to scattering from the microcrack porosity (Mason and McSkimin, 1947; Yamakawa, 1962). These pressure-dependent variations of the apparent Q further illustrate the nonstationarity of the waveforms. Indeed, only above pressures of 150 MPa does Q exhibit a nearly constant value with pressure. Consequently, at low confining pressure, picking nonstationary features of the waveforms such as a first peak can yield ambiguous results, and the traveltimes so measured have no clear, consistent meaning. Similarly, crosscorrelation between a reference and such nonstationary sample waveforms introduces additional traveltime errors which directly affect the determination of velocity.

One valid criticism of rock-core measurements is that they can never provide the true intrinsic velocity of the multiphase material because of the existence of microcrack porosity. This is particularly true in more brittle igneous and metamorphic rocks (e.g., Meglis et al., 1996) or in highly consolidated calcareous rock (e.g., Schmitt and Li, 1996). It is difficult or impossible to gauge at which point the microcrack porosity in such

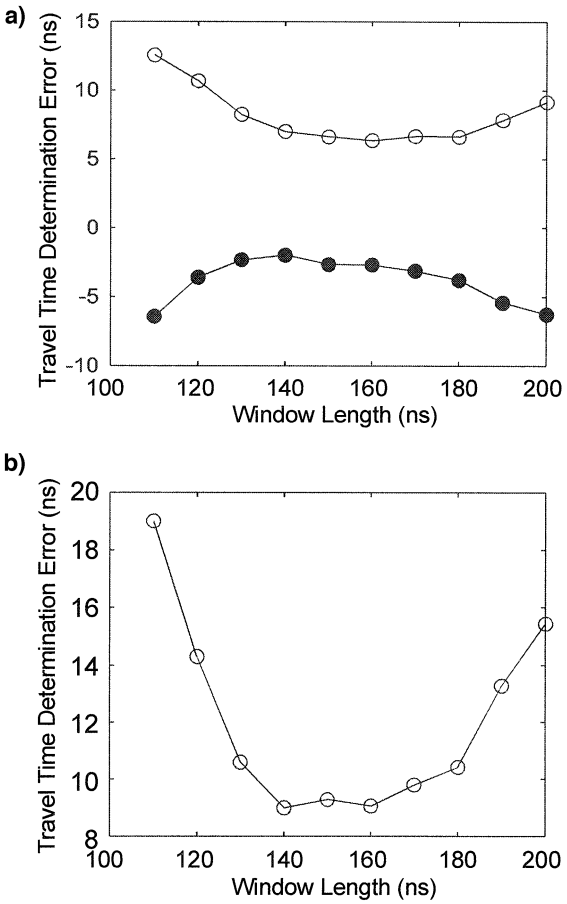

FIG. 7. The effect of template length on picking accuracy for the synthetic data set. (a) Mean transit time determination error (solid circles) and standard deviation (open circles) versus template length. Negative relative time picks indicate the Pearson correlation method picks are slightly delayed with respect to the true onset of the signal. (b) Traveltime error (addition of standard deviation and mean magnitudes) versus window length.

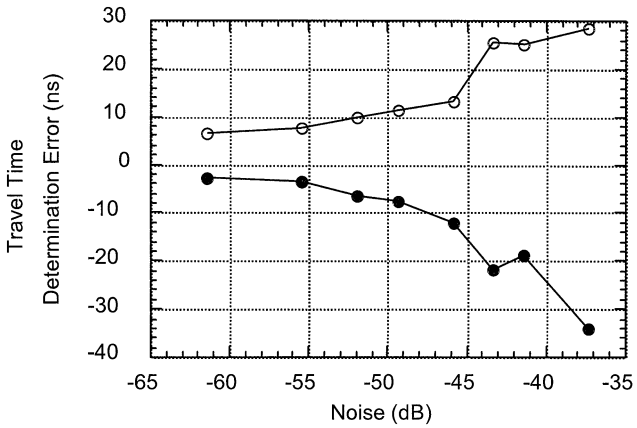

FIG. 8. Mean transit time determination error (solid circles) and its standard deviation (open circles) versus level of added noise.

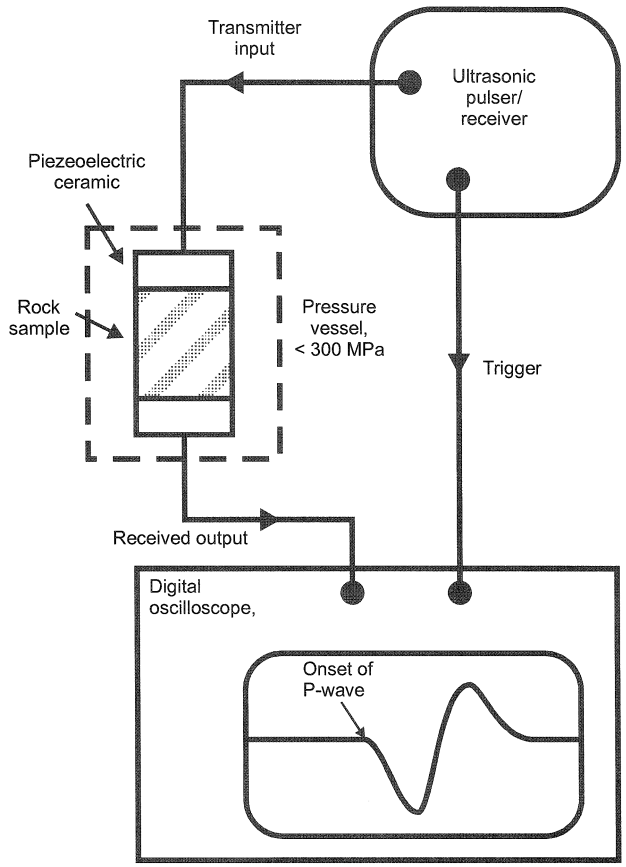

FIG. 9. Simplified experimental configuration.

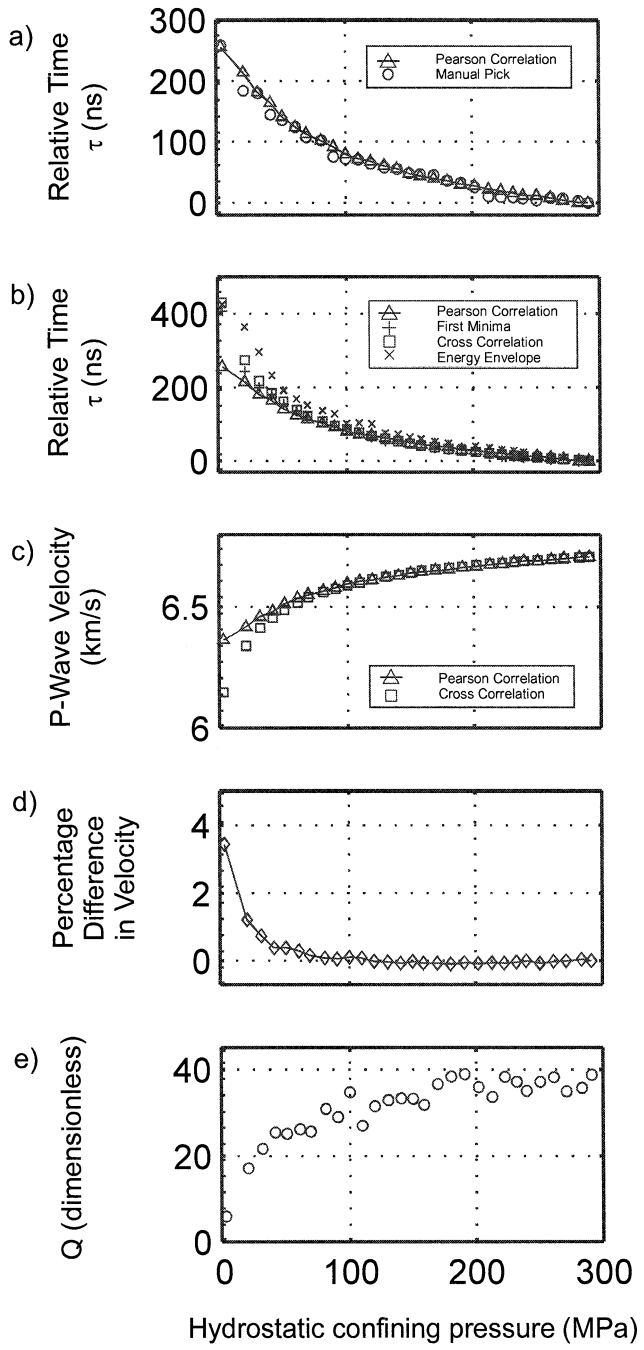

FIG. 10. Pressure- and method-dependent measures of transit time, velocity, and attenuation. (a) Manually picked (circles) and Pearson regression onset traveltimes (triangles with a background solid line) relative to the 290-MPa reference versus confining pressure. (b) Pearson regression onset (triangles), first-amplitude minima (crosses), waveform crosscorrelation (squares), and amplitude envelope crosscorrelation (x's) transit times relative to the 290-MPa reference versus confining pressure. (c) Velocities derived using Pearson regression onset (triangles) and waveform crosscorrelation (squares) transit times versus confining pressure. (e) Differences in the velocities in (d) expressed as a percentage of the Pearson regression velocity versus confining pressure. (e) Apparent quality factor Q versus confining pressure.

rocks is closed. Workers have usually assumed that the velocity versus pressure graph becomes linear once most the cracks are closed. Further pressure-dependent velocity increases result primarily from the smaller changes in the intrinsic elastic moduli. The results of Figures 10d and 10e suggest that leveling the time difference between the signal onset and crosscorrelation times and the Q value versus pressure provides additional criteria toward the evaluation of intrinsic velocity measurements. Leveling these measures indicates stationarity of the waveforms, which in turn suggests that the general state of the material remains unaltered to the highest pressures in the experiment.

CONCLUSIONS

The traveltimes of the onset arrival of ultrasonic pulses transmitted through core samples were determined to within 0.3% by a direct correlation method for our data with −60 dB of noise. This time uncertainty compares well with the 2% error commonly quoted in laboratory pulse transmission methods. Essentially, the onset segment of the time series is correlated with a suitable reference that can either be a similar waveform or an appropriate quadratic function. Substantial differences of up to 4% in the velocities determined using the onset and other criteria were found in the laboratory data set used, indicative of velocity dispersion.

The method described requires a template wavelet, with a manually picked first break, to compare to all other first breaks. A fully automated procedure, without the need for a manual pick, could be used by running a series of slightly different quadratic templates in the Pearson picking scheme. The templates yielding the best correlation would provide an absolute traveltime.

The direct correlation method was developed for use in highly time-resolved, low-noise signals acquired in the laboratory. Tests on synthetic data have shown 60-ns errors for −37 dB noise levels (1.2% velocity error). This is equivalent to an average mispick of 1 data point for seismic data sampled at 2 ms, with a dominant frequency of 60 Hz. This moderate error suggests that the Pearson correlation method may be applicable to determine onset traveltimes in other dispersive-velocity environments in which noise levels are moderate: full-waveform sonic logging, high-frequency crosshole tomography, and VSP first-break identification.

Finally, there are relatively large discrepancies observed between velocities determined using the onset and other traveltime determination criteria. This suggests that care should be taken by experimentalists in the laboratory and the field in describing how traveltime delays, and hence velocities, are measured in attenuating media. This is particularly critical when conditions such as confining stress, pore pressure, and saturation state influence the attenuation characteristics of the material. Experimental work in progress seeks to better understand the link between velocity measurement and attenuation.

ACKNOWLEDGMENTS

The authors acknowledge the aid of R. Hunt, J. Haverstock, B. Madu, L. Tober, and the anonymous reviewers. This work

was supported by grants provided by NSERC, LITHOPROBE Supporting Science, and PanCanadian Petroleum. Discussions with P. Blenis were appreciated. LITHOPROBE contribution #984.

REFERENCES

Birch, F., 1960, The velocity of compressional waves in rocks to 10 kilobars, part 1: J. Geophys. Res., **65**, 1083–1102.

——— The velocity of compressional waves in rocks to 10 kilobars, part 2: J. Geophys. Res., **66**, 2199–2224.

Boschetti, F., Denitith, M. D., and List, R. D., 1996, A fractal-based algorithm for detecting first arrivals on seismic traces: Geophysics, **61**, 1095–1102.

Bourbie, T., and Zinszner, B., 1987, Hydraulic and acoustic properties as a function of porosity in Fountainbleau sandstone: J. Geophys. Res., **90**, 11 524–11 542.

Brillouin, L., 1960, Wave propagation and group velocity: Academic Press Inc.

Christiansen, N. I., 1965, Compressional wave velocities in metamorphic rocks at pressure to 10 kilobars: J. Geophys. Res., **70**, 6147–6164.

Coppens, F., 1985, First arrival picking on common-offset trace collections for automatic estimation of static corrections: Geophys. Prosp., **33**, 1212–1231.

Ervin, C., McGinnis, L. D., Otis, R. M., and Hall, M. L., 1983, Automated analysis of marine refraction data: Geophysics, **48**, 582–589.

Fountain, D. M., Salisbury, M. H., and Percival, J. A., 1990, Seismic structure of the continental crust based on rock velocity measurements from the Kapuskasing uplift: J. Geophys. Res., **95**, 1167–1186.

Futterman, W., 1962, Dispersive body waves: J. Geophys. Res., **67**, 5279–5291.

Ganley, D. C., and Kanasewich, E. R., 1980, Measurement of absorption and dispersion from check shot surveys: Geophysics, **85**, 5219–5226.

Gelchinsky, B., and Shtivelman, V., 1986, Automatic picking of first arrivals and parameterization of travel time curves: Geophys. Prosp., **31**, 915–928.

Gudmundsson, O., 1996, On the effect of diffraction on travel time measurements: Geophys. J. Internat., **124**, 304–314.

Hajnal, Z., Lucas, S., White, D., Lewry, J., Besdan, S., Stauffer, M. R., and Thomas, M. D., 1996, Seismic reflection images of high-angle faults and linked detachments in the Trans-Hudson orogen: Tectonics, **15**, 427–439.

Hatherly, P. J., 1982, A computer method for determining seismic first arrival times: Geophysics, **47**, 1431–1436.

Kebaili, A., and Schmitt, D. R., 1996, Velocity anisotropy observed in wellbore seismic arrivals: Geophysics, **61**, 12–20.

Kern, H., and Richter, A., 1981, Temperature derivatives of compressional and shear wave velocities in crustal and mantle rocks at 6 Kbar confining pressure: J. Geophys. Res., **49**, 47–56.

King, M. S., 1966, Wave velocities in rocks as a function of changes in overburden pressure and pore fluid saturation: Geophysics, **31**, 50–73.

Mason, W. P., and McSkimin, H. J., 1947, Attenuation and scattering of high frequency sound waves in metals and glasses: J. Acoust. Soc. Am., **19**, 454–473.

Meglis, I. L., Greenfield, R. J., Engelder, T., and Graham, E. K., 1996, Pressure dependence of velocity and attenuation and its relationship to crack closure in crystalline rocks: J. Geophys. Res., **101**, 17 523–17 533.

Murat, M., and Rudman, A., 1992, Automated 1st arrival picking: Geophys. Prosp., **40**, 587–604.

Papadakis, E. P., 1990, The measurement of ultrasonic velocity: Phys. Acoust., **19**, 81–105.

Peraldi, R., and Clement, A., 1972, Digital processing of refraction data study of first arrivals: Geophys. Prosp., **20**, 529–548.

Ramananantoandro, R., and Beritsas, N., 1987, A computer algorithm for automatic picking of refraction first-arrival time: Geoexploration, **34**, 147–151.

Ricker, N., 1953, The form and laws of propagation of seismic wavelets: Geophysics, **18**, 10–40.

Schmidt, T., and Muller, G., 1986, Seismic signal velocity in absorbing media: J. Geophys., **60**, 199–203.

Schmitt, D. R., and Li, Y., 1996, Three dimensional stress relief displacements from drilling a blind hole: Experiment. Mech., **36**, 412–420.

Spagnolini, U., 1991, Adaptive picking of refracted first arrivals: Geophys. Prosp., **39**, 293–312.

Su, W., and Dziewonski, A. M., 1992, On the scale of mantle heterogeneity: Phys. Earth Plan. Int., **74**, 29–54.

Taner, M. T., Koehler, F., and Sheriff, R. E., 1979, Complex seismic trace analysis: Geophysics, **44**, 1041–1063.

Taylor, J. R., 1982, An introduction to error analysis: Univ. Science Books.

Toksoz, M. N., Johnston, D. H., and Timur, A., 1979, Attenuation of seismic waves in dry and saturated rocks: I, Laboratory measurements: Geophysics, **44**, 681–690.

Yamakawa, N., 1962, Scattering and attenuation of elastic waves: Geophys. Magazine, Tokyo, **31**, 63–103.

Zamanek, J., Jr., and Rudnick, J., 1961, Attenuation and dispersion of elastic waves in a cylindrical bar: J. Acoust. Soc. Am., **23**, 1283–1288.